

Supplementary Materials for

A continental system for forecasting bird migration

Benjamin M. Van Doren* and Kyle G. Horton

*Corresponding author. Email: benjamin.vandoren@zoo.ox.ac.uk

Published 14 September 2018, *Science* **361**, 1115 (2018)

DOI: 10.1126/science.aat7526

This PDF file includes:

Materials and Methods
Figs. S1 to S10
References

Materials and Methods

Doppler radar

We used the NEXRAD network operated by the National Oceanic and Atmospheric Administration to characterize spring migratory movements (March 1st to May 31st) from 1995 to 2017. These radars scan 360° at multiple elevation angles (e.g. 0.5°, 1.5°... 4.5°), fully sampling the airspace every 5 to 10 minutes. We downloaded radar scans from Amazon Web Services (<https://s3.amazonaws.com/noaa-nexrad-level2/index.html>), selecting those in a 30-minute window centered on three hours after local sunset. We chose this time window because it approximates the time of peak nocturnal migration across the United States (e.g., 3, 25). However, there is spatial variation in the time of peak nocturnal migration (e.g., stations along the Gulf of Mexico experience peak migration earlier in the night, 26), so in some areas our predicted totals will be conservative. We processed scans using the WSRLIB weather surveillance radar package for MATLAB (27). To characterize migration intensity, we used radar reflectivity factor, a measure of reflectance to the radar. To sample the airspace from 0-3 km above ground level, we extracted radar reflectivity factor values 5-37.5km from each radar (28) and cast them into vertical profiles with 100-m altitudinal resolution. We converted radar reflectivity factor (dBZ) to radar reflectivity (dB η) using the equation $\eta[\text{dB}] = Z[\text{dBZ}] + \beta$, where $\beta = 10\log_{10}(10^3\pi^5|K_m|^2/\lambda^4)$. We set the radar wavelength (λ) to 10.71 cm, the average for NEXRAD radars (16) and set the refractive index ($|K_m|^2$) to 0.93 for liquid water. This yielded $\beta = 13.35$. We converted dB η to η using the equation $\eta = 10^{dB\eta/10}$, yielding units of $\text{cm}^2\text{km}^{-3}$. To estimate numbers of birds from η , we divided η by a radar cross-section of 11 cm^2 . This resulted in units of birds km^{-3} .

To mitigate the influence of time-invariant clutter (e.g., buildings, terrain, wind turbines), we applied binary clutter masks to each low elevation scan prior to the construction of the vertical profile of migration intensity. Masks were generated by summing a minimum of 100 low elevation scans (0.5° elevation), starting on January 1st (16:00 UTC to 18:00 UTC) and continuing to January 15th. This time window falls well outside typical migration periods. If 100 samples were not tallied by January 15th, the window of selection was expanded until the threshold was met. We classified any pixel above the 85th percentile of the summed reflectivity as clutter and masked it from our calculation of migration intensity.

To discriminate radar scans contaminated with precipitation from those containing only clear air or bird-dominated signal (hereafter termed “clear”), we created a random forest classifier using the package “randomForest” (29). We trained the classifier on 157,279 manually classified nocturnal scans (generated every 5-10 minutes) selected from a 3-hour period on March 15th, April 15th, and May 15th for every radar and every year in the training set (fig. S8). We designed this sampling to capture any geographic, seasonal, or longitudinal patterns in the data. We extracted derived predictor variables from profiles of radar reflectivity, groundspeed, and summaries of the number of density values above 35 dBZ (extreme densities characteristic of intense precipitation). We generated 1,000 trees and set the minimum terminal node size to 50. Overall, the model showed a 5.6% classification error. We used the algorithm to classify a total of 979,326 scans. As an additional step to reduce the inclusion of precipitation incorrectly classified as clear, we used only scans with a probability of being clear >70% (rather than a majority rule, i.e. >50%).

Identifying and removing flying insects from weather surveillance radar data has been a long-standing challenge for ornithologists. The standard method of ameliorating insect

contamination is to filter data by airspeed values, because samples with large average airspeeds must be dominated by strong flyers (30, 31). One downside to this approach is that it may also remove samples containing slow-flying birds or a mix of birds and insects. Here, we filter vertical profiles by removing altitude bins with mean airspeeds of 5 m s^{-1} or less (3, 22, 32), a cutoff value chosen to remove the majority of insects (30, 33). Slow-flying samples represented 16% of total summed reflectivity. We examined the sensitivity of our analysis to this step by comparing model predictions with and without insect filtering (fig. S9).

Weather reanalysis

The North American Regional Reanalysis, or NARR (19), compiles data from numerous observational data sources to produce a best estimate of weather conditions that occurred in North America. The reanalysis is published in 3-hour intervals across a 32-km grid. We downloaded NARR data for 1995-2017 and extracted the following parameters: air temperature ($^{\circ}\text{C}$), geopotential height (m), zonal and meridional wind components (m s^{-1}), surface pressure (Pa), relative humidity (%), visibility (m), vertical velocity (Pa s^{-1}), mean sea level pressure (Pa), total cloud cover (%), albedo (%), total precipitation (kg m^{-2}), convective available potential energy (J kg^{-1}), and snow cover (%). For variables available at multiple pressure levels, we extracted data from the surface to 300 mb. To match weather data to radar stations, we averaged data within 37.5 km of each radar station. We then calculated altitude above ground level by subtracting surface geopotential height from the geopotential height at each pressure level, and we used linear interpolation to calculate vertical profiles of weather data at 100-m altitude bins from 0-3000 m. Finally, we matched radar profiles to weather profiles by taking the observation closest in time for each radar station. Pairwise correlations among predictor variables were generally low (fig. S1).

Weather forecasts

The North American Mesoscale Forecast System, or NAM (<https://www.ncdc.noaa.gov/data-access/model-data/model-datasets/north-american-mesoscale-forecast-system-nam>), generates weather forecasts out to 84 hours; forecasts are hourly from 1-36 hours and subsequently every 3 hours until hour 84. Forecast models are run every 6 hours. NAM predictions are made on a 12-km grid. We downloaded 0Z NAM forecast data for 2008-2017, extracted the same parameters as for NARR, and matched NAM data to radar stations in the same manner as for NARR.

In addition to NAM, we used the Global Forecast System, or GFS (<https://www.ncdc.noaa.gov/data-access/model-data/model-datasets/global-forecast-system-gfs>) to generate longer-range migration forecasts. GFS forecasts with 0.5° spatial resolution currently extend out to 384 hours at 3-hour increments, but this range has improved with time; in 2010, the range was 180 hours. We downloaded 0Z GFS forecast data for 2010-2017 and extracted weather predictions up to 7 days (168 h) in advance.

Supervised learning

We used gradient boosted trees to predict bird migration from weather data (Fig. 1). We used the R implementation of XGBoost (18, 34), a highly efficient and scalable gradient boosting framework. The algorithm automatically detects nonlinear effects and complex interactions among predictors, and it is not hindered by predictor collinearity. We trained an XGBoost model on NARR weather data, with the cube root of bird density as our response variable.

5

We divided our dataset into three groups: a training set, for learning; a validation set, for hyperparameter tuning; and a test set, to evaluate performance. We split the dataset by whole days instead of individual data points to prevent any spatial autocorrelation from inflating performance metrics. From 2,115 total days (comprising 3,434,703 altitude bins across 143 radar stations after filtering steps), we randomly selected 75% of days for training, 10% for validation, and 15% for testing.

We tuned model hyperparameters with grid searches across hyperparameter space (fig. S10). For our first search, we set the learning rate *eta* to 0.05 while varying maximum tree depth *max_depth* between 8-16. Trees of these depths are complex, but predicting bird migration across the entire United States from March to May at 30 different altitude bins is a complex problem. We used the *early_stopping_rounds* argument to stop the algorithm after 10 boosting iterations in which performance on the validation set failed to improve. Larger trees perform better on training data, but trees that are too large lower performance due to overfitting. We therefore used the validation dataset to select the best-performing value of maximum tree depth. We then tested the following modifications to additional parameters that can prevent overfitting: decreasing *subsample* from 1.0 to 0.70, increasing *min_child_weight* from 1 to 5, and increasing *gamma* from 0 to 1 or 10. We tried all 12 combinations of these modifications. The best combination of parameters was the following: *max_depth* = 12, *min_child_weight* = 5, *gamma* = 1, *colsample_bytree* = 1, and *subsample* = 0.7. Using the best combination of hyperparameters, we further lowered the learning rate to 0.01 and set *early_stopping_rounds* to 100 to determine the optimal number of boosting iterations for that learning rate. Lower learning rates decrease the contribution of each tree to the model, making the boosting algorithm more conservative and further preventing overfitting, but lower learning rates require more iterations. With this information, we fit a final model with learning rate = 0.01 on the combined training and validation sets. We then evaluated its performance on the test dataset (15% of data), which had been withheld from all training and validation. To assess performance, we calculated two metrics: root mean square error and the coefficient of determination (or R^2). We calculated R^2 by dividing the sum of squared errors by the total sum of squares, and then subtracting this value from 1. An R^2 value of 0 indicates that the model does not explain the data any better than a simple null model that predicts the mean for each observation, while a negative R^2 value indicates that the model explains the data worse than this null model.

25

In an XGBoost model, correlated or uninformative predictors generally have little negative effect; they will generally not be incorporated during tree construction. However, extraneous predictors increase computational time and data storage requirements, making the forecast system more unwieldy to operationalize. For this reason, we sought to remove uninformative predictors. Using the *xgboost* package, we calculated the gain, a predictor importance metric that quantifies how much a tree improves by adding a split on a given variable. Gain values are scaled to sum to 1. After the first grid search step, we identified and eliminated predictors with gain values less than 0.01 and restarted the tuning procedure. In this manner, we eliminated albedo, vertical velocity, convective available potential energy, total precipitation, and snow cover. This left 12 variables in the final model: ordinal date, height above ground level, latitude, longitude, air temperature, relative humidity, zonal wind, meridional wind, surface pressure, mean sea level pressure, visibility, and total cloud cover.

35

We trained and tested two further modifications to the final model: one which also included additional conditions variables from the previous night (winds, temperature, and surface pressure) and their 24-hour changes, and another which included these lagged weather variables

plus migration intensity measured during the previous night. Our aim here was to determine how much additional explanatory power we could achieve with a model that took into account recently observed conditions and behavior.

5 Performance and importance

To assess performance of the final model using weather forecasts instead of reanalysis (i.e. NARR) data, we tested the model using archived NAM forecasts made 1-3 days in advance. We did the same for GFS forecasts made 1-7 days in advance. Because GFS does not contain a visibility variable, we first retrained the model without visibility included in order to conduct this evaluation.

10 To assess model performance at unobserved spatial locations, we performed a cross-validation where we randomly removed one station (out of 143 total) from the dataset, retrained the model on the remaining data, and tested its performance on the withheld station.

15 We identified the predictor variables that were most important for model predictions using gain, a measure of the variable's importance in making accurate predictions. We also generated partial dependence plots using the R package *mlr* (35) to explore how these variables influence predictions. Here, we used a learning rate *eta* of 0.05 instead of 0.01 to make computation tractable.

20 Prediction intervals

We constructed empirical prediction intervals using residuals from XGBoost predictions for the validation dataset. We fitted a generalized additive model (36) on squared XGBoost residuals against the XGBoost-predicted value to account for an error variance that increased with the magnitude of the predicted value. The generalized additive model produced an estimated error variance for each predicted value, which we used to construct 90% prediction intervals using 0.05/0.95 Gaussian quantiles. We constructed separate models for upper and lower limits to allow for asymmetry in the width of the interval, and we used the Gamma distribution family in the generalized additive model to constrain the predicted variances to be non-negative.

30 Forecast output and estimation of nightly migration magnitude

Using our validated migration forecast model, we made predictions across the entire 12-km NAM grid. For smooth presentation, we averaged predictions across 9×9 cell blocks. We also used our model to estimate the total number of birds migrating over the continental United States each night. For this we used the NARR dataset because it is the best retrospective estimate of occurred conditions. For each 32-km NARR grid cell covering the continental United States, we multiplied the bird density estimate by the area of the cell and summed totals across all grid cells for each night.

40 NEXRAD radars operate at slightly different carrier frequencies (and hence different wavelengths) to reduce interference from neighboring radars, and this variation may introduce noise into estimates of total bird numbers if radars differ substantially in wavelength (37). However, such noise is likely to be minor because (1) most radars operate at more similar wavelengths than the example presented in (37), (2) variation in carrier frequency is not correlated with geography (i.e. no consistent spatial bias would be introduced), and (3) including wavelength as a model predictor to account for any systematic difference in detected bird densities did not appreciably change model performance.

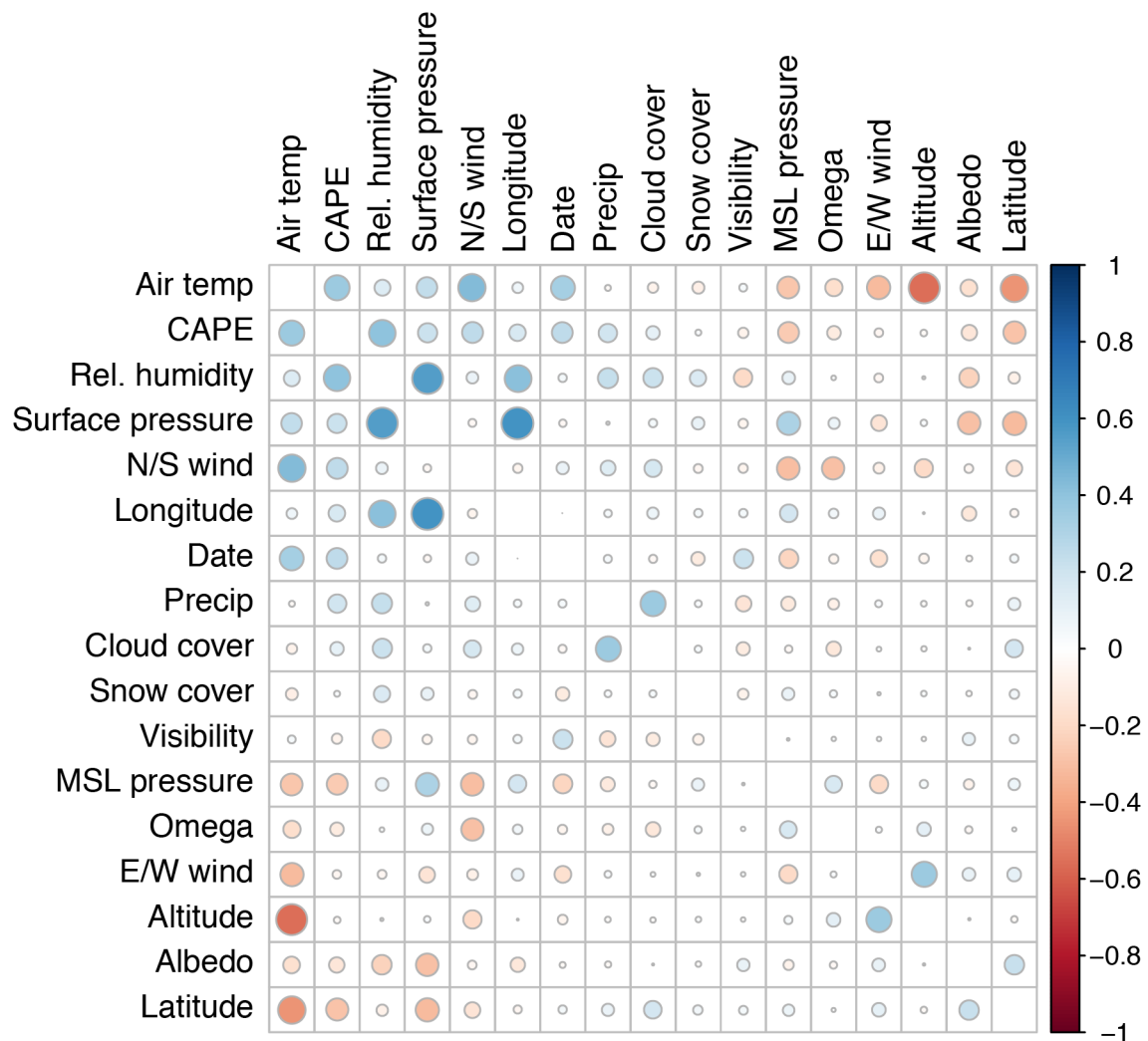


Fig. S1. Spearman rank correlations among all pairs of predictor variables. No pair of predictors had absolute Spearman or Pearson correlation coefficients greater than 0.60.

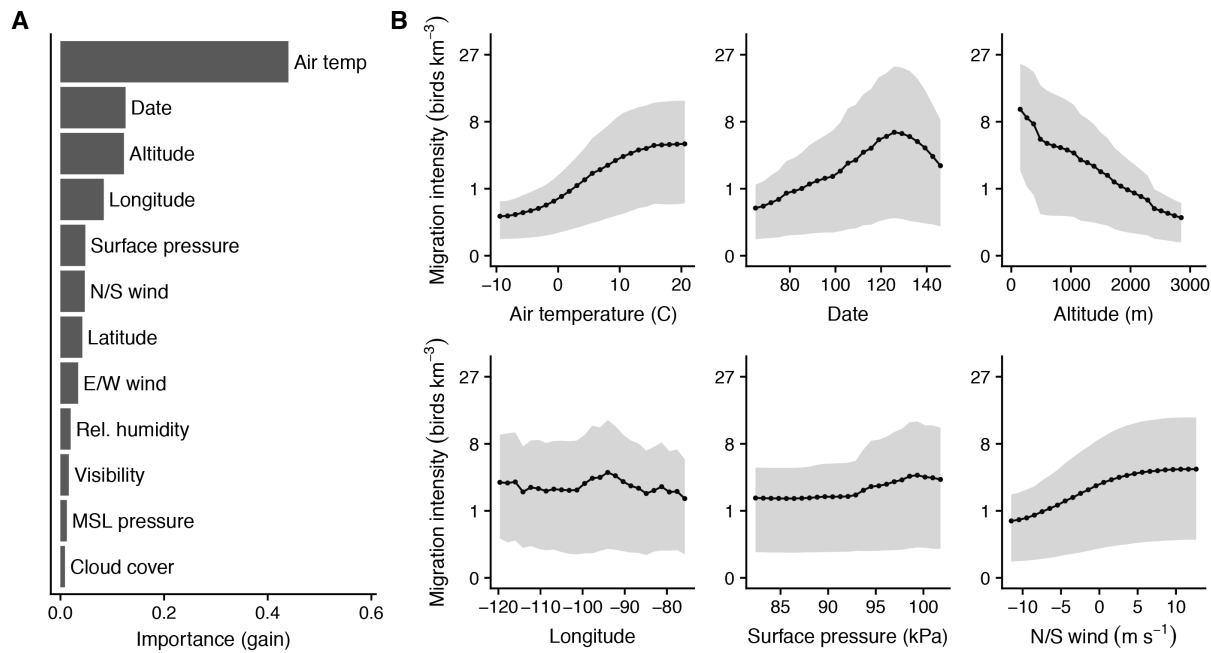


Fig. S2. Predictor importance and partial dependence. (A) Predictor importance measured by gain. Gain is a measure of each variable's importance in making accurate predictions. (B) One-dimensional partial dependence plots for the six most important predictor variables. Solid lines show the mean and shading shows the middle 50% of predicted y-values. Note that this is not a confidence interval; it shows the marginal distribution of y-values over the values of all other predictors and should be expected to be wider than confidence limits. Narrower shading indicates that the predictor explains a greater proportion of variance in the predicted values.

5

10

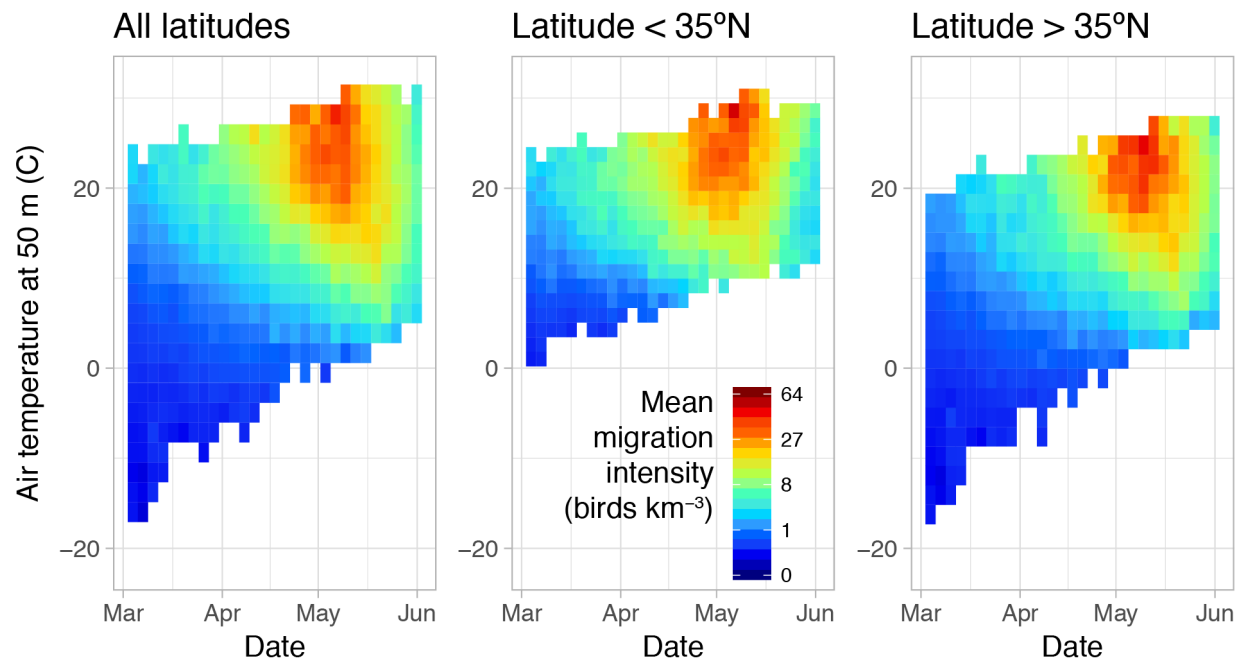


Fig. S3. Mean observed migration intensity by date and temperature close to surface. For a given date, the highest migration intensities occurred where temperatures close to the surface were warmest, especially at higher latitudes. This figure summarizes raw data and does not show model output.

5

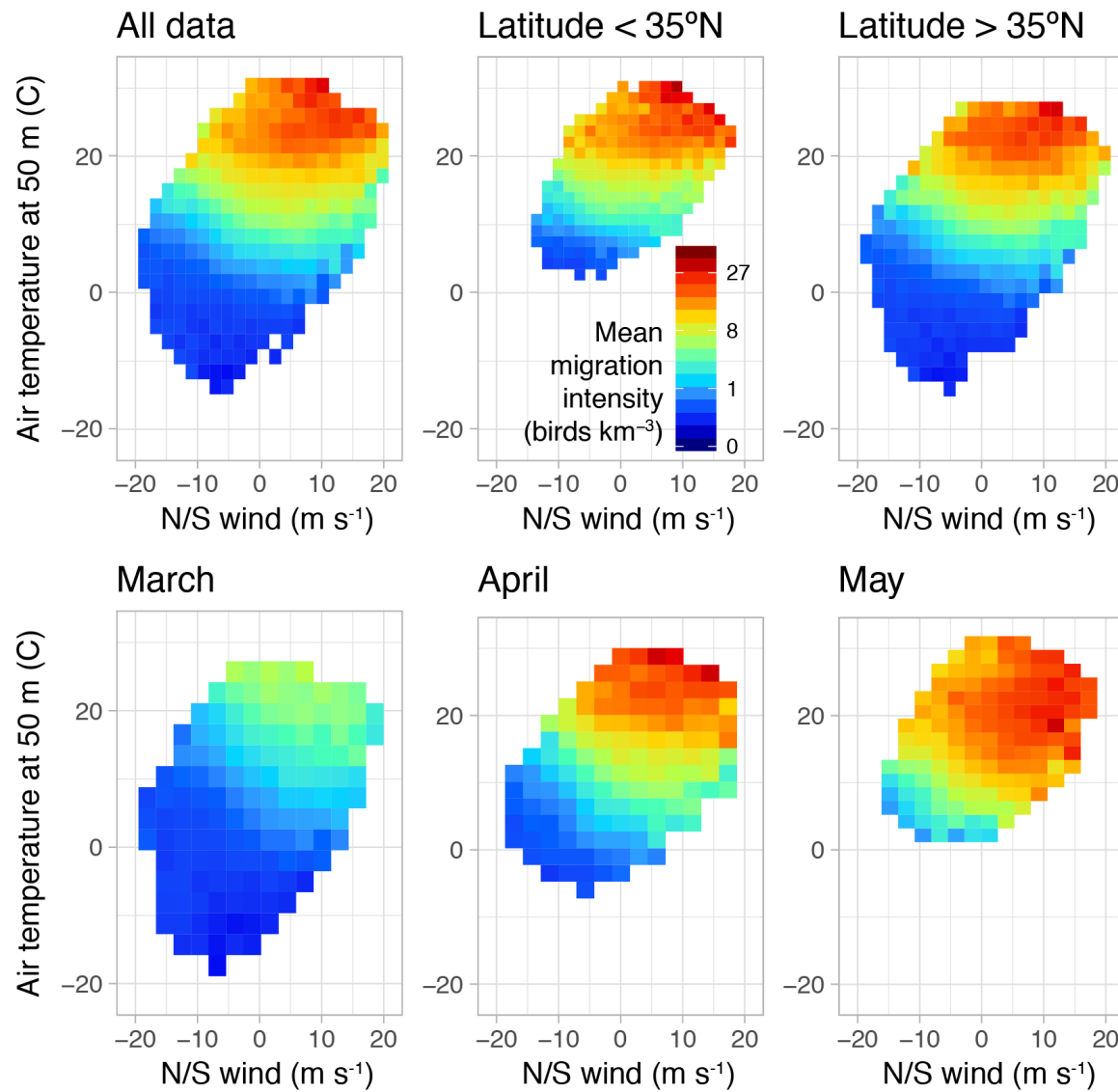


Fig. S4. Mean observed migration intensity by temperature close to the surface and wind direction. For given wind conditions, the highest migration intensities occurred where temperatures close to the surface were warmest, especially at higher latitudes. This figure summarizes raw data and does not show model output.

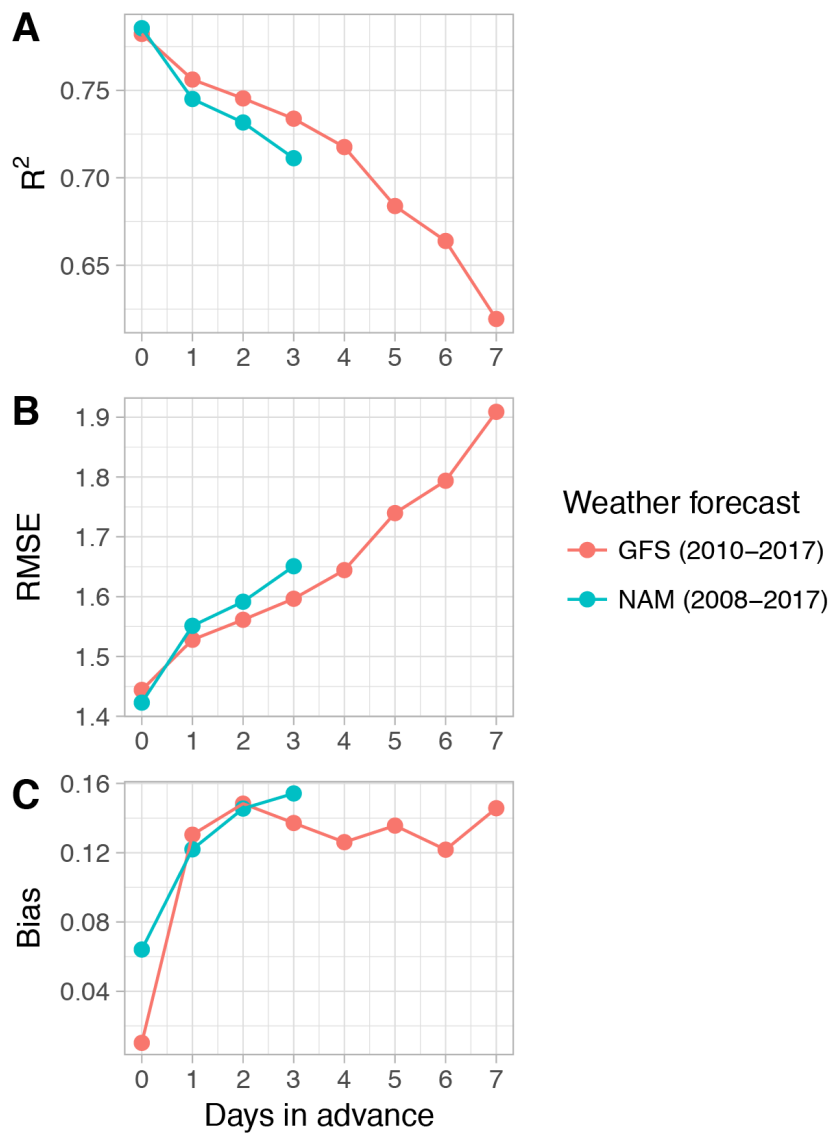


Fig. S5. Model performance using weather forecast data. We evaluated performance on the test dataset using the Global Forecast System (GFS) and North American Mesoscale (NAM) forecast system.

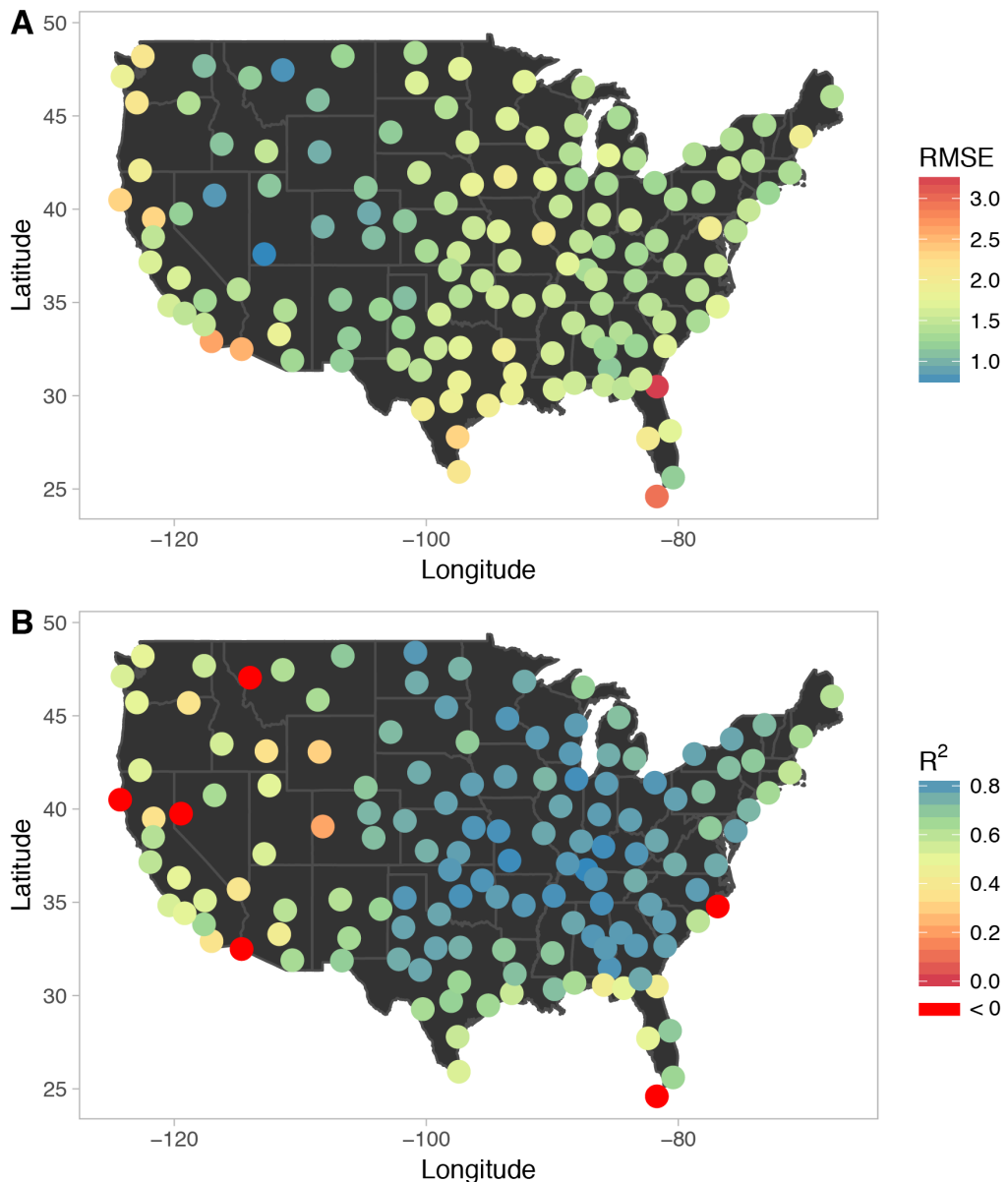


Fig. S6. Relative and absolute performance at radar stations withheld from the training dataset. Performance was best at interior sites, especially in the central and eastern United States. At a small minority (4%) of withheld sites, relative performance was poor ($R^2 < 0$, indicating performance was worse than a naive model that predicts the mean response for each observation), which may be due to local influences such as topography (e.g. see Florida Keys).

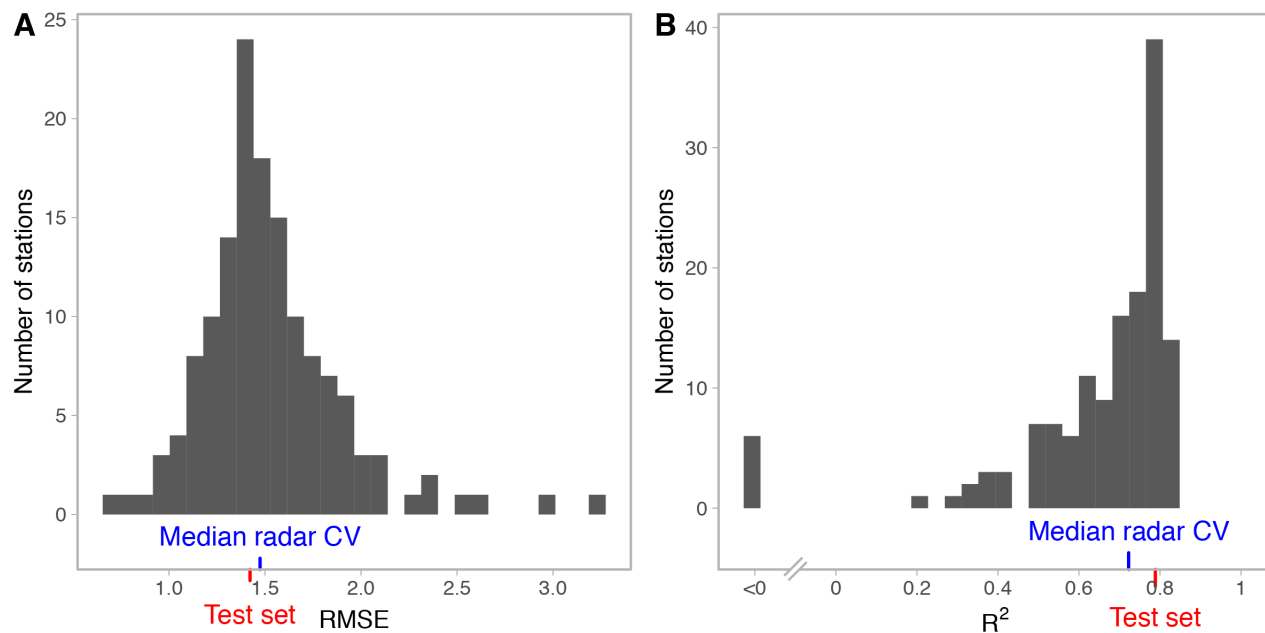


Fig. S7. Model performance at unobserved locations. Histograms show the distribution of (A) absolute and (B) relative performance metrics for radar stations that were withheld from the training dataset. The blue tick marks show the median value across sites, and the red tick marks show the corresponding value for the randomly-selected test set (all locations included).

5

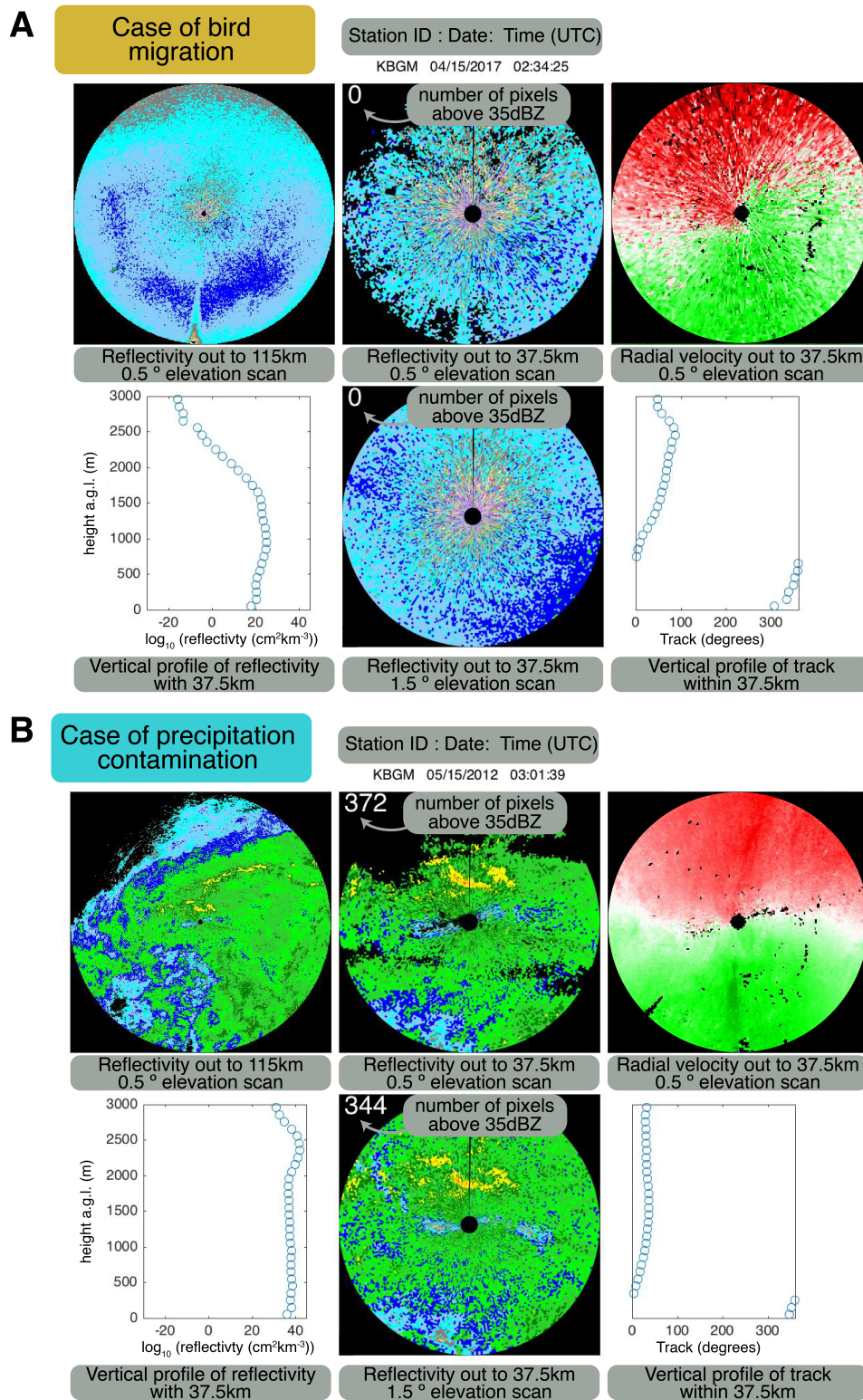


Fig. S8. Composite images used for classifying radar scans containing precipitation. Panels show example cases of (A) bird migration and (B) precipitation contamination.

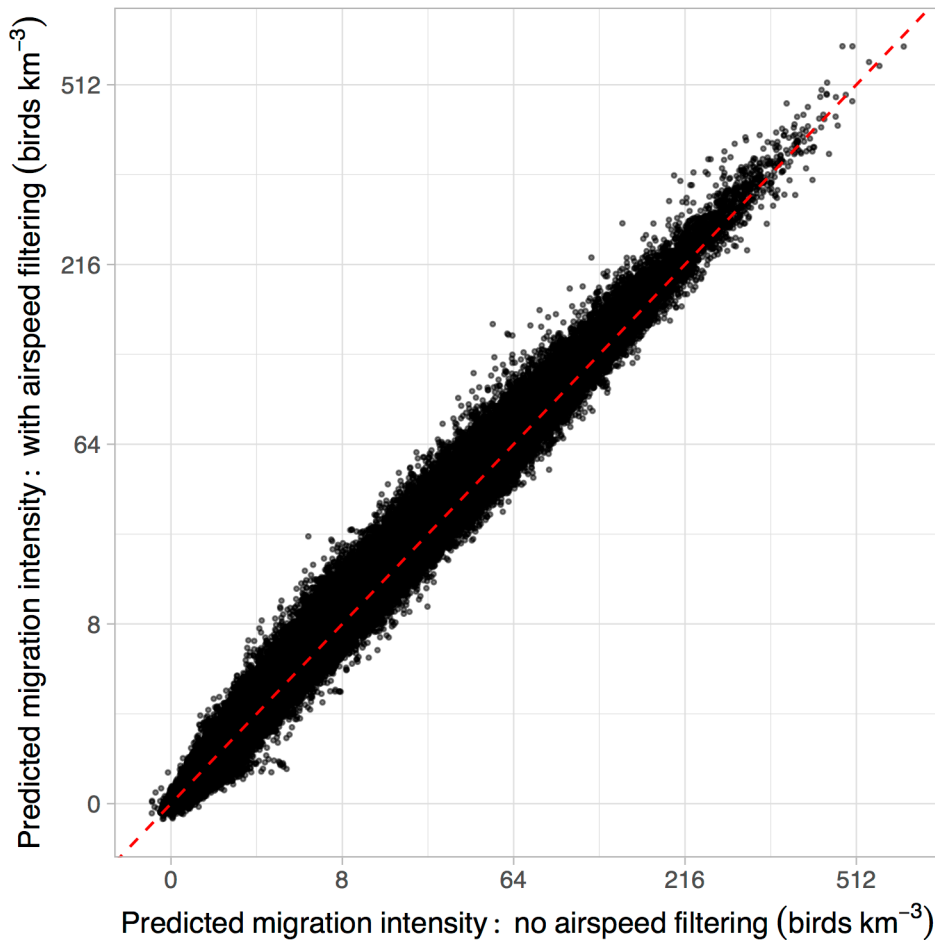


Fig. S9. Model results are robust to possible insect contamination. We removed altitude bins with mean airspeed $\leq 5 \text{ m s}^{-1}$ to limit the inclusion of flying insects in our dataset. Predictions made by a model trained without airspeed filtering corresponded closely to those made by the final model with airspeed filtering (Pearson's $r = 0.995$). Prediction error for these two models was comparable (RMSE = 1.422 with filtering; RMSE = 1.442 without filtering). The dashed red line is the identity line.

10

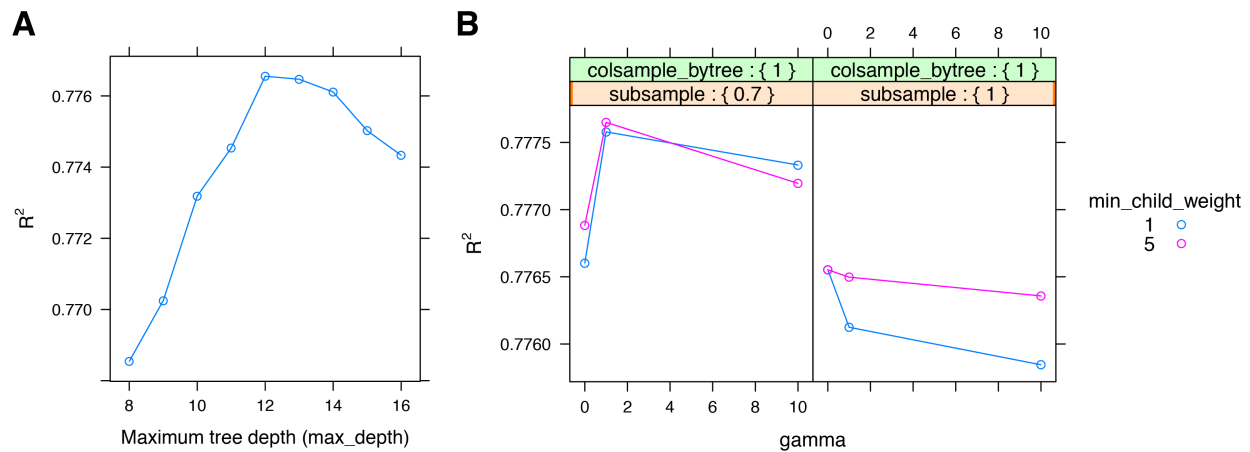


Fig. S10. Hyperparameter tuning using validation dataset. (A) We first varied maximum tree depth, and second (B) varied three parameters that may aid in limiting overfitting. Note that hyperparameter tuning affected performance only to a small degree (~1% in A and ~0.3% in B).

5

References and Notes

1. S. R. Loss, T. Will, P. P. Marra, Direct mortality of birds from anthropogenic causes. *Annu. Rev. Ecol. Evol. Syst.* **46**, 99–120 (2015). [doi:10.1146/annurev-ecolsys-112414-054133](https://doi.org/10.1146/annurev-ecolsys-112414-054133)
2. J. D. McLaren, J. J. Buler, T. Schreckengost, J. A. Smolinsky, M. Boone, E. Emiel van Loon, D. K. Dawson, E. L. Walters, Artificial light at night confounds broad-scale habitat use by migrating birds. *Ecol. Lett.* **21**, 356–364 (2018). [doi:10.1111/ele.12902](https://doi.org/10.1111/ele.12902) Medline
3. A. Farnsworth, B. M. Van Doren, W. M. Hochachka, D. Sheldon, K. Winner, J. Irvine, J. Geevarghese, S. Kelling, A characterization of autumn nocturnal migration detected by weather surveillance radars in the northeastern USA. *Ecol. Appl.* **26**, 752–770 (2016). [doi:10.1890/15-0023](https://doi.org/10.1890/15-0023) Medline
4. B. Erni, F. Liechti, L. Underhill, B. Bruderer, Wind and rain govern the intensity of nocturnal bird migration in central Europe—a log-linear regression analysis. *Ardea* **90**, 155–166 (2002).
5. B. M. Van Doren, K. G. Horton, A. M. Dokter, H. Klinck, S. B. Elbin, A. Farnsworth, High-intensity urban light installation dramatically alters nocturnal bird migration. *Proc. Natl. Acad. Sci. U.S.A.* **114**, 11175–11180 (2017). [doi:10.1073/pnas.1708574114](https://doi.org/10.1073/pnas.1708574114) Medline
6. W. J. Richardson, Timing and amount of bird migration in relation to weather: A review. *Oikos* **30**, 224–272 (1978). [doi:10.2307/3543482](https://doi.org/10.2307/3543482)
7. F. Liechti, Birds: Blowin' by the wind? *J. Ornithol.* **147**, 202–211 (2006). [doi:10.1007/s10336-006-0061-9](https://doi.org/10.1007/s10336-006-0061-9)
8. M. U. Kemp, J. Shamoun-Baranes, A. M. Dokter, E. van Loon, W. Bouten, The influence of weather on the flight altitude of nocturnal migrants in mid-latitudes. *Ibis* **155**, 734–749 (2013). [doi:10.1111/ibi.12064](https://doi.org/10.1111/ibi.12064)
9. S. A. Gauthreaux, *Direct Visual and Radar Methods for the Detection, Quantification, and Prediction of Bird Migration* (Department of Zoology, Clemson University, 1980).
10. J. Van Belle, J. Shamoun-Baranes, E. Van Loon, W. Bouten, An operational model predicting autumn bird migration intensities for flight safety. *J. Appl. Ecol.* **44**, 864–874 (2007). [doi:10.1111/j.1365-2664.2007.01322.x](https://doi.org/10.1111/j.1365-2664.2007.01322.x)
11. S. A. Gauthreaux, C. G. Belser, D. van Blaricom, “Using a network of WSR-88D weather surveillance radars to define patterns of bird migration at large spatial scales,” in *Avian Migration*, P. Berthold, E. Gwinner, E. Sonnenschein, Eds. (Springer, 2003), pp. 335–346.
12. A. M. Dokter, F. Liechti, H. Stark, L. Delobbe, P. Tabary, I. Holleman, Bird migration flight altitudes studied by a network of operational weather radars. *J. R. Soc. Interface* **8**, 30–43 (2011). [doi:10.1098/rsif.2010.0116](https://doi.org/10.1098/rsif.2010.0116) Medline
13. G. Hu, K. S. Lim, N. Horvitz, S. J. Clark, D. R. Reynolds, N. Sapir, J. W. Chapman, Mass seasonal bioflows of high-flying insect migrants. *Science* **354**, 1584–1587 (2016). [doi:10.1126/science.aah4379](https://doi.org/10.1126/science.aah4379) Medline

14. T. Alerstam, G. A. Gudmundsson, M. Green, A. Hedenström, Migration along orthodromic sun compass routes by arctic birds. *Science* **291**, 300–303 (2001).
[doi:10.1126/science.291.5502.300](https://doi.org/10.1126/science.291.5502.300) [Medline](#)
15. J. F. Kelly, K. G. Horton, Toward a predictive macrosystems framework for migration ecology. *Glob. Ecol. Biogeogr.* **25**, 1159–1165 (2016). [doi:10.1111/geb.12473](https://doi.org/10.1111/geb.12473)
16. T. D. Crum, R. L. Alberty, The WSR-88D and the WSR-88D operational support facility. *Bull. Am. Meteorol. Soc.* **74**, 1669–1687 (1993). [doi:10.1175/1520-0477\(1993\)074<1669:TWATWO>2.0.CO;2](https://doi.org/10.1175/1520-0477(1993)074<1669:TWATWO>2.0.CO;2)
17. D. R. Sheldon, A. Farnsworth, J. Irvine, B. M. Van Doren, K. F. Webb, T. G. Dietterich, S. Kelling, “Approximate Bayesian inference for reconstructing velocities of migrating birds from weather radar,” in *Proceedings of the Twenty-Seventh AAAI Conference on Artificial Intelligence*, M. des Jardins, M. L. Littman, Eds. (Association for the Advancement of Artificial Intelligence, 2013), pp. 1334–1340.
18. T. Chen, C. Guestrin, “XGBoost: A Scalable Tree Boosting System,” in *Proceedings of the 22nd ACM SIGKDD International Conference on Knowledge Discovery and Data Mining* (Association for Computing Machinery, 2016), pp. 785–794.
19. F. Mesinger, G. DiMego, E. Kalnay, K. Mitchell, P. C. Shafran, W. Ebisuzaki, D. Jović, J. Woollen, E. Rogers, E. H. Berbery, M. B. Ek, Y. Fan, R. Grumbine, W. Higgins, H. Li, Y. Lin, G. Manikin, D. Parrish, W. Shi, North American Regional Reanalysis. *Bull. Am. Meteorol. Soc.* **87**, 343–360 (2006). [doi:10.1175/BAMS-87-3-343](https://doi.org/10.1175/BAMS-87-3-343)
20. A. Aurbach, B. Schmid, F. Liechti, N. Chokani, R. Abhari, Complex behaviour in complex terrain—modelling bird migration in a high resolution wind field across mountainous terrain to simulate observed patterns. *J. Theor. Biol.* **454**, 126–138 (2018).
[doi:10.1016/j.jtbi.2018.05.039](https://doi.org/10.1016/j.jtbi.2018.05.039) [Medline](#)
21. S. Bauer, J. W. Chapman, D. R. Reynolds, J. A. Alves, A. M. Dokter, M. M. H. Menz, N. Sapir, M. Ciach, L. B. Pettersson, J. F. Kelly, H. Leijnse, J. Shamoun-Baranes, From agricultural benefits to aviation safety: Realizing the potential of continent-wide radar networks. *Bioscience* **67**, 912–918 (2017). [doi:10.1093/biosci/bix074](https://doi.org/10.1093/biosci/bix074) [Medline](#)
22. K. G. Horton, B. M. Van Doren, F. A. La Sorte, D. Fink, D. Sheldon, A. Farnsworth, J. F. Kelly, Navigating north: How body mass and winds shape avian flight behaviours across a North American migratory flyway. *Ecol. Lett.* **21**, 1055–1064 (2018).
[doi:10.1111/ele.12971](https://doi.org/10.1111/ele.12971) [Medline](#)
23. J. Shamoun-Baranes, H. van Gasteren, V. Ross-Smith, “Sharing the aerosphere: Conflicts and potential solutions,” in *Aeroecology*, P. Chilson, W. F. Frick, J. Kelly, F. Liechti, Eds. (Springer, 2017), pp. 465–497.
24. B. M. Van Doren, K. G. Horton, Dataset for “A continental system for forecasting bird migration,” figshare (2018); <https://doi.org/10.6084/m9.figshare.6962810>.
25. K. G. Horton, W. G. Shriner, J. J. Buler, A comparison of traffic estimates of nocturnal flying animals using radar, thermal imaging, and acoustic recording. *Ecol. Appl.* **25**, 390–401 (2015). [doi:10.1890/14-0279.1](https://doi.org/10.1890/14-0279.1) [Medline](#)

26. S. A. Gauthreaux Jr., A radar and direct visual study of passerine spring migration in southern Louisiana. *Auk* **88**, 343–365 (1971). [doi:10.2307/4083884](https://doi.org/10.2307/4083884)
27. D. Sheldon, WSRLIB: MATLAB Toolbox for Weather Surveillance Radar; <https://bitbucket.org/dsheldon/wsrlib>.
28. K. G. Horton, B. M. Van Doren, P. M. Stepanian, W. M. Hochachka, A. Farnsworth, J. F. Kelly, Nocturnally migrating songbirds drift when they can and compensate when they must. *Sci. Rep.* **6**, 21249 (2016). [doi:10.1038/srep21249](https://doi.org/10.1038/srep21249) Medline
29. A. Liaw, M. Wiener, Classification and regression by randomForest. *R News* **2/3**, 18–22 (2002).
30. S. A. Gauthreaux Jr., C. G. Belser, Displays of bird movements on the WSR-88D: Patterns and quantification. *Weather Forecast.* **13**, 453–464 (1998). [doi:10.1175/1520-0434\(1998\)013<0453:DOBMOT>2.0.CO;2](https://doi.org/10.1175/1520-0434(1998)013<0453:DOBMOT>2.0.CO;2)
31. S. A. Cabrera-Cruz, T. J. Mabee, R. V. Patraca, Using theoretical flight speeds to discriminate birds from insects in radar studies. *Condor* **115**, 263–272 (2013). [doi:10.1525/cond.2013.110181](https://doi.org/10.1525/cond.2013.110181)
32. K. G. Horton, B. M. Van Doren, P. M. Stepanian, A. Farnsworth, J. F. Kelly, Seasonal differences in landbird migration strategies. *Auk* **133**, 761–769 (2016). [doi:10.1642/AUK-16-105.1](https://doi.org/10.1642/AUK-16-105.1)
33. R. P. Larkin, Flight speeds observed with radar, a correction: Slow “birds” are insects. *Behav. Ecol. Sociobiol.* **29**, 221–224 (1991). [doi:10.1007/BF00166405](https://doi.org/10.1007/BF00166405)
34. T. Chen, T. He, M. Benesty, V. Khotilovich, Y. Tang, *xgboost: eXtreme Gradient Boosting* (R Foundation, 2017).
35. B. Bischl, M. Lang, L. Kotthoff, J. Schiffner, J. Richter, E. Studerus, G. Casalicchio, Z. M. Jones, *mlr: Machine learning in R*. *J. Mach. Learn. Res.* **17**, 1–5 (2016).
36. S. N. Wood, *Generalized Additive Models: An Introduction with R* (Chapman and Hall/CRC, ed. 2, 2017).
37. V. M. Melnikov, R. R. Lee, N. J. Langlieb, Resonance effects within S-band in echoes from birds. *IEEE Geosci. Remote Sens. Lett.* **9**, 413–416 (2012). [doi:10.1109/LGRS.2011.2169933](https://doi.org/10.1109/LGRS.2011.2169933)